# FABRICATION AND CHARACTERIZATION OF PZT–PMnN–PSbN CERAMICS DOPED WITH ZnO

**Nguyen Truong Tho[1]\*, Le Dai Vuong[2]**

[1] University of Sciences, Hue University, 77 Nguyen Hue St., Hue, Vietnam
[2] Faculty of Chemical and Environmental Engineering, Hue Industrial College, 70 Nguyen Hue St., Hue, Vietnam

\* Correspondence to Nguyen Truong Tho <ntthokh@hueuni.edu.vn>

**Abstract.** The effect of the ZnO addition to the pure perovskite PZT–PMnN–PSbN ceramics sintered at 950–1200 °C was investigated. The phase structure of ceramics changes from rhombohedral to tetragonal, and the sintering temperature decreases with the increase of the ZnO content. The limited $Zn^{2+}$ concentration for its solubility in PZT–PMnN–PSbN systems is about 0.25% wt. At this concentration, the ceramic exhibits a density of 8.20 $g/cm^3$ and dielectric constants of 1,555 for $\varepsilon_p$ and 32,900 for $\varepsilon_{max}$. The highest value of $\varepsilon_{max}$ (about 22,000) was found at 1 kHz at $T_m$ around 575 K. The diffuse phase transition was determined by using the extended Curie–Weiss law. Cole–Cole analyses show the non-Debye-type relaxation in the system.

**Keywords:** perovskite, ceramics, PZT–PMnN–PSbN, diffuse phase transition, Cole–Cole analyses

## 1    Introduction

During the last several decades, the relaxor ferroelectrics have been extensively studied since their discovery by Smolenskii et al. [1], owing to their significant technical importance on the application to electromechanical devices, such as multilayer ceramic capacitors, electrostrictive transducers, and micro–displacement positioners. Recently, there have been studies on lead-free ferroelectric materials to overcome lead toxicity [2-4]. However, their physical properties are not sufficiently suitable to replace the role of Pb in ferroelectric materials [5-11]. Therefore, in addition to continuing research on lead-free ferroelectric materials, further improvement of the physical properties of Pb-related materials is necessary.

As Pb(Mn_{1/3}Nb_{2/3})O_3 (PMnN) and Pb(Sn_{1/3}Nb_{2/3})O_3 (PZN) are members of lead-based relaxor ferroelectric family with different cations

on the B-site of perovskite lattice, they are ferroelectric materials with a high dielectric constant, broad temperature range of diffuse phase transition, and strong frequency dependency of dielectric properties. So far, the sintering temperature of PZT-based ceramics is usually very high, approximately 1200 °C [12-15]. To reduce the temperature, at which satisfactory densification could be obtained, various material processing methods, such as the 2-stage calcination [16], high-energy mill [17], and liquid-phase sintering [14-16, 18-20], have been performed. Among these methods, liquid-phase sintering is an effective technique for aiding the densification of specimens at low sintering temperatures.

Perovskite-based relaxor ferroelectric materials have generated considerable interest due to the wide diversity of their physical properties and possible applications in various technologies like memory storage devices, micro-electro-

mechanical systems, multilayer ceramic capacitors, and recently, in the area of optoelectronic devices [13-15]. It occupies a particular place among the complex oxides $A(B'_mB''_{1-m})O_3$ with promising dielectric properties. In contrast to normal ferroelectrics, they exhibit a strong frequency dispersion of the dielectric constant without the change in crystalline phase structure in the temperature region near $T_m$ (the temperature, at which the diffuse permittivity is given maximum). Basically, in compositionally homogenous systems, the quenched random disorder breaks the long-range polar order in the unit cell level, leading to the broadening of $\varepsilon'(T)$ [16]. Such materials exhibit relatively slow relaxation dynamics and hence have been termed ferroelectric relaxors [16, 17]. Burns and Decol [18] observed the existence of polar-regions in the relaxor at temperatures higher than $T_m$. In principle, the relaxors are classified into two families: the first is the lead manganese niobate (PMN) 1:2 family, such as $Pb(Mg_{1/3}Nb_{2/3})O_3$, and the second is the lead scandium niobate (PSN) 1:1 family, such as $Pb(Sc_{1/2}Nb_{1/2})O_3$.

In the ceramics $PZT–Pb(Mg_{1/3}Nb_{2/3})O_3$ and $PZT–Pb(Zn_{1/3}Nb_{2/3})O_3$ systems, belonging to the first family and $PT–Pb(Sc_{1/2}Nb_{1/2})O_3$, belonging to the second family, the dielectric transition complies with the extended Curie-Weiss law. The results of study in these systems indicate that the dielectric relaxation is the non-Debye type [19, 21].

In this study, we investigate the effect of ZnO on the sintering behavior and physical properties of the PZT–PMnN–PSbN ceramics. We report the dielectric behavior of PZT–PMnN–PSbN + $x$% wt. ZnO ceramics that are given by the combination of a normal ferroelectric with two above relaxor families. The real and imaginary parts of the dielectric permittivity and loss dielectric in a frequency range of 0.1–500 kHz at a temperature range of 270–320 °C are analyzed.

We investigate the diffuse phase transition of the system by using the extended Curie–Weiss law and determine the parameters in this relation by fitting.

## 2    Experimental

### 2.1    Samples preparation

PZT–PMnN–PSbN + $x$% (wt) ZnO ceramics were prepared from reagent-grade raw-material oxides via the columbite and wolframite method to suppress the formation of the pyrochlore phase. The chemicals used in the study are as follows: PbO (Merck, 99.0%), $ZrO_2$ (SEPR, 99.5%), $TiO_2$ (Merck, 99.6%), $MnCO_3$ (Merck, 99.5%), $Nb_2O_5$ (Merck, 99.5%) and $Sb_2O_3$ (SEPR, 99.6%). The synthesis was carried out in three steps:

*Step 1*: To synthesise $MnNb_2O_6$ and $Sb_2Nb_2O_8$, $MnCO_3$, $Nb_2O_5$, $Sb_2O_3$, and $Nb_2O_5$ were mixed and acetone-milled for 20 h in a zirconia ball mill and then calcined at 1250 °C for 3 h to form $MnNb_2O_6$ and $Sb_2Nb_2O_8$. The material was acetone-ground for 10 h in the mill and dried again.

*Step 2*: To synthesise PZT–PMnN–PSbN calcined powders, reagent-grade PbO, $ZrO_2$, and $TiO_2$ were mixed with $MnNb_2O_6$ and $Sb_2Nb_2O_8$ powders in a ball mill for 20 h in acetone. The mixed powders were dried and calcined at 850 °C for 2 h and then ground in the mill in acetone for 24 h.

*Step 3*: To synthesise PZT–PMnN–PSbN + $x$% wt. ZnO ceramics, the PZT–PMnN–PSbN calcined powders were mixed with ZnO ($x$ = 0.05, 0.15, 0.2, 0.25, 0.30, 0.40, and 0.50, and the samples were designated as Z05, Z10, Z15, Z20, Z25, Z30, Z40, and Z50, respesively), acetone-milled for 8 h in the zirconia ball mill and then dried.

The ground materials were pressed into disks of 12 mm in diameter and 1.5 mm in thickness under 100 MPa. The samples were sintered at 850, 900, 950, 1000, and 1050 °C for 3 h

in an alumina crucible to form the ZnO-doped PZT–PMnN–PSbN ceramics. The sintered and annealed samples were ground and cut to 1 mm in thickness. A silver electrode was fired at 500 °C for 10 minutes on the major surface of the samples. Poling was performed in the direction of thickness in a silicon oil bath under 30 kV/cm for 15 minutes at 120 °C.

## 2.2 Microstructure, dielectric properties measurement

The bulk densities of sintered specimens were measured by using the Archimedes technique. The crystalline phase was analyzed with an *X*-ray diffractometer (XRD). The microstructure of the sintered bodies was examined with a scanning electron microscope (SEM). The grain size was measured by using the line intercept method. The dielectric permittivity and dielectric dissipation of samples were measured on a highly automatized RLC HIOKI 3532 at 1 kHz.

## 3 Results and discussion

### 3.1 Effect of ZnO addition on sintering behavior of PZT–PMnN–PSbN ceramics

It can be seen that the density of PZT–PMnN–PSbN ceramics changes as a function of sintering temperature and the content of ZnO (Fig. 1). Without ZnO, sufficient densification occurs at temperatures 1250 °C. Meanwhile, ZnO enables the ceramic samples to densify at a temperature as low as 950 °C (7.82 g/cm$^3$ at 0.25% wt. ZnO), indicating its usefulness to lower the sintering temperature of the ceramics. This finding is consistent with that of other reports on ZnO-added PZT-based ceramics [13-15]. When the amount of ZnO increases from 0.05 to 0.25% wt., the density of the samples increases with the increasing amount of ZnO and the sintering temperature and then decreases.
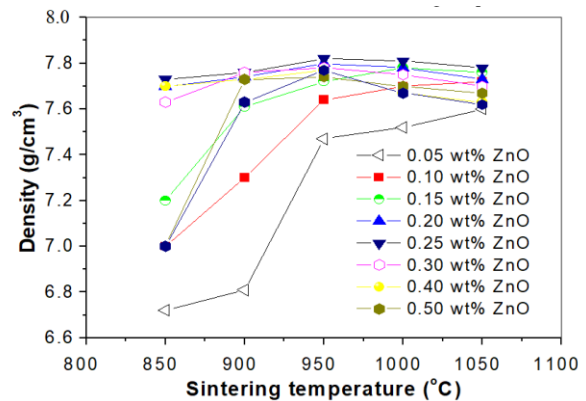


**Fig. 1.** Density of PZT–PMnN–PSbN + *x*% wt. ZnO ceramics as function of sintering temperature

According to the above results, the optimized sintering temperature of the ZnO-doped PZT–PMnN–PSbN ceramics is 950 °C. Thus, the addition of ZnO improves the sinterability of the samples and causes an increase in the density at low sintering temperatures.

### 3.2 Effect of ZnO addition on structure and microstructure of PZT–PMnN–PSN ceramics

Fig. 2 shows the X-ray diffraction patterns (XRD) of the PZT–PMnN–PSbN ceramics at different contents of ZnO. All samples have a pure perovskite phase, and the phase structure of ceramics changes from rhombohedral to tetragonal with the increase of the ZnO content.

Fig. 3 shows the SEM micrographs of the fractured surface of the ZnO-added PZT–PMnN–PSbN specimens sintered at 950 °C for 2 h. The sintering-aid-added PZT–PMnN–PSbN specimens show a uniform and densified structure. In the ZnO-added PZT–PMnN–PSbN systems, the low-temperature sintering mechanism primarily originates from transition liquid-phase sintering. In the early and middle stages of the sintering process, ZnO with a low melting point forms a liquid phase, which wets and covers the surface of the grains and facilitates the dissolution and migration of the species.
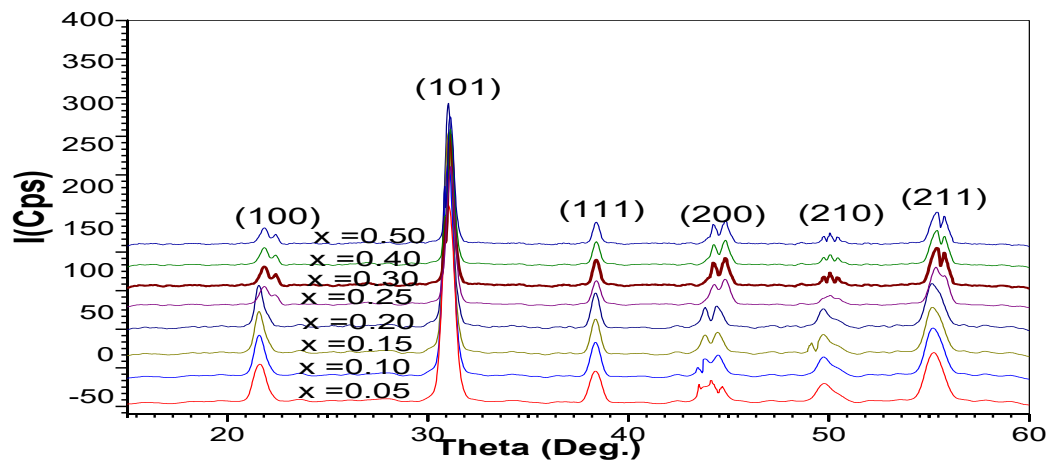
**Fig. 2.** X-ray diffraction patterns of ceramics with different ZnO contents
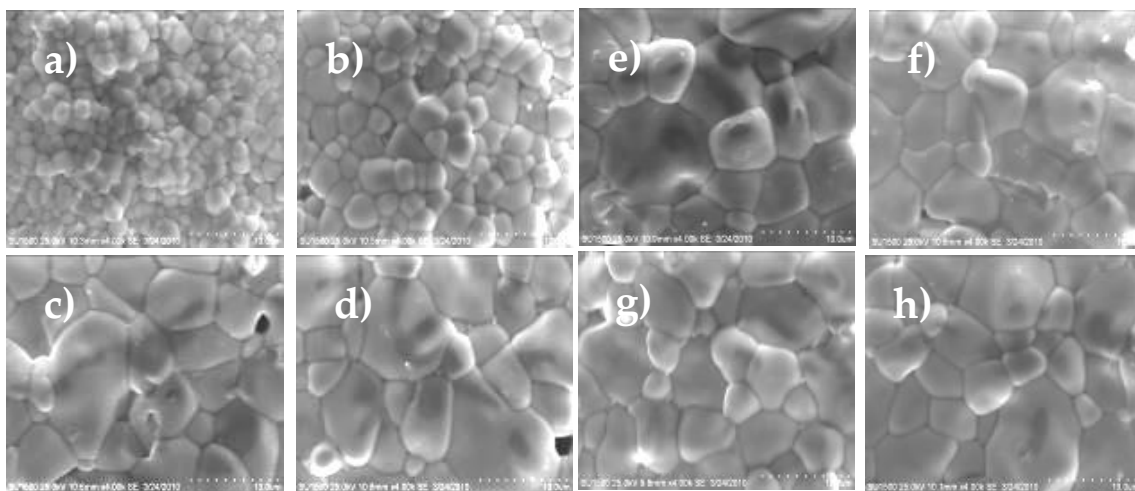


**Fig. 3.** SEM micrographs of fractured surface of PZT–PMnN–PSbN specimens with different contents of ZnO (% wt.): a) 0.05, b) 0.1, c) 0.15, d) 0.2, e) 0.25, f) 0.3, g) 0.4, and h) 0.5

### 3.3 Effect of ZnO addition on diffuse phase transition of PZT–PMnN–PSbN system

Fig. 4 presents the temperature dependence of the real ($\varepsilon'$) and imaginary ($\varepsilon''$) part of the dielectric constant and loss tangent ($\tan\delta$) of the PZT–PMnN–PSbN ceramics at 1 kHz. The dielectric permittivity maximum ($\varepsilon'_{max}$) and its temperature ($T_m$) are listed in Table 1. As seen in Fig. 4, the dielectric properties exhibit the characteristics of a relaxor material, in which the phase transition temperature occurs within a broad range. This is one of the characteristics of

ferroelectrics with disordered perovskite structure [22]. The origin of the disorder is caused by variation in the local electric field, variation in the local strain field, and the formation of vacancies in the crystalline structure of the materials. A random local electric field resulting from different valences of B-site cations and a variation of the local strain field due to the difference in the radius of the B-site cation [22]. For the PZT–PMnN–PSbN system, the B-site is occupied by $Zn^{2+}$, $Mn^{2+}$, $Sb^{3+}$, $Nb^{5+}$, $Zr^{4+}$, and $Ti^{4+}$. Thus, the degree of disorder in this system is mainly caused by the difference of valences of $Zn^{2+}$ with $Zr^{4+}/Ti^{4+}$.
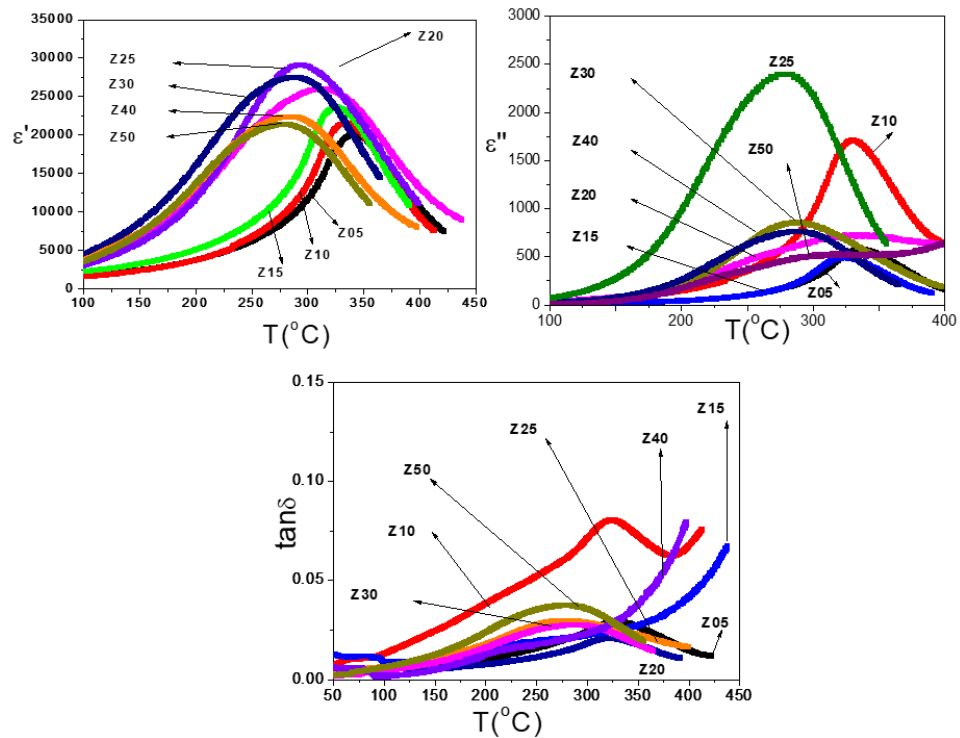
**Fig. 4.** Temperature dependence of real (ε′), imaginary (ε′′) parts of dielectric constant and loss tangent (tanδ) of PZT-PMnN-PSbN + $x$% wt. ZnO ceramics at 1 kHz

The value of $T_m$ decreases with the increasing ZnO content while that of ε′$_{max}$ is maximum at Z25 (0.25% wt. ZnO). This may be because the Curie temperature reflects the stability of the B-site ions in the oxygen octahedron, which can be determined from the formation energy of octahedra. Therefore, the substitution of B-site $Zr^{4+}$ or $Ti^{4+}$ ion with $Zn^{2+}$ can decrease the stability of the B-site ion in the octahedra.

It is observed that the temperature of maximum permittivity of all samples ($T_m$) shifts to higher values while ε$_{max}$ decreases and (tanδ)$_{max}$ increases upon increasing frequency. Fig. 4 also shows that all samples have a diffuse phase transition in the transition temperature region.

The real (ε′) and imaginary (ε′′) part of the dielectric constant and loss tangent (tanδ) can be calculated from the measured capacitance and phase values of the samples versus temperature. The maximum dielectric permittivity (ε′$_{max}$) at 1 kHz, its temperature ($T_m$), and the fitting parameters calculated by using the modified Curie–Weiss law are listed in Table 1. The value of $T_m$ increases with increasing PMnN component, but the ε′$_{max}$ abnormally depends on the ZnO component and has a maximum value at $x$ = 0.25.
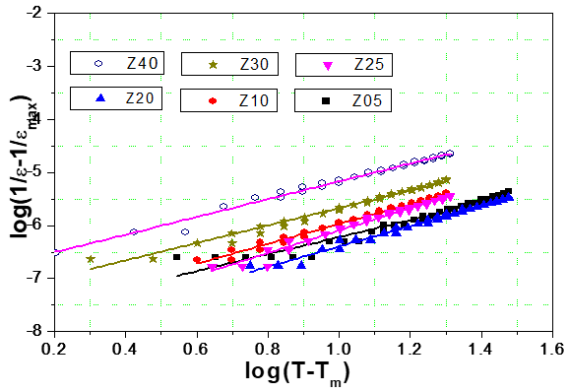
In order to examine the diffuse phase transition and relaxor properties, the following modified Curie–Weiss formula was used for analyzing experimental data:

$$\frac{1}{\varepsilon} - \frac{1}{\varepsilon_{max}} = \frac{(T - T_m)^\gamma}{C'} \tag{1}$$

or

$$\log\left(\frac{1}{\varepsilon} - \frac{1}{\varepsilon_{max}}\right) = \gamma\log(T - T_m) - \log C' \tag{2}$$

where $C'$ is the modified Curie–Weiss constant, and $\gamma$ is the diffuseness exponent, which changes from 1 to 2 for normal ferroelectrics to fully disorder relaxor ferroelectrics, respectively. Eq. (1) can be solved graphically by using a log-log plot, as shown in Fig. 5.

**Fig. 5.** Dependence of $\log(1/\varepsilon - 1/\varepsilon_{max})$ on $\log(T - T_m)$ for Z25 sample at 1 kHz

The given value of $\gamma$ at 1 kHz, presented in Table 1 is the evidence to suggest that the diffuse phase transition (DPT) takes place in the samples. It is expected that the disorder in the cation distribution (compositional fluctuations) causes the transition, in which the local Curie points of different micro-regions are statistically distributed in a wide temperature range around the mean Curie point. The non-equality of phase transition temperature obtained from $\varepsilon(T)$ and $\tan\delta(T)$ measurement also confirms the existence of the transition. It has shown that the value of the diffuseness, $\gamma$, increases with increasing ZnO component, resulting in an increase in the disorder in the B-site of the materials .

A common characteristic of all relaxors is the existence of disorder in the crystalline structure. In principle, the disorder is caused by the variation in the local electric field as well as in the local strain field related to the formation of vacancies in the crystalline structure of the materials and/or with the different valences and radius of the B-site cation [20]. For the PZT–PMnN–PSbN system, the B-site is occupied by $Mn^{2+}$, $Sb^{3+}$, $Nb^{5+}$, $Zr^{4+}$, and $Ti^{4+}$. Both $Mn^{2+}$ and $Sb^{3+}$ have the ionic radii rather similar: 0.08 nm for $Mn^{2+}$ and 0.082 nm for $Sb^{3+}$, as substituted on $Nb^{5+}$ (0.069 nm), $Zr^{4+}$ (0.079 nm), or $Ti^{4+}$ (0.068 nm), and $Zn^{2+}$ (0.099 nm) [19]. Thus, the degree of disorder in this system is mainly caused by the difference of valences of $Zn^{2+}$, $Mn^{2+}$, and $Sb^{3+}$ with $Zr^{4+}/Ti^{4+}$.

Fig. 6 presents the Curie-Weiss dependence $1/\varepsilon'$ of the Z25 sample. It is clearly seen that at the temperature region far above $T_m$, the dependence fits well to a linear line. This dependence indicates the appearance of the paraelectric phase in the sample. The linear line cut the $1/\varepsilon - T$ curve at a point called Burns temperature $T_B$, the temperature at which the disorder nanoclusters start to appear with cooling down the sample. The values of $T_B$ derived from fitting are also presented in Table 1. The obtained results suggest that in the diffuse phase transition materials, the ferroelectric disorder nanoclusters could exist in a temperature region much higher than the $T_C$ evaluated from the Curie–Weiss relationship.

**Table 1.** Dielectric permittivity maximum ($\varepsilon'_{max}$) and its temperature ($T_m$), and the fitting parameters to the modified Curie–Weiss law

| Sample | $\varepsilon$ | $\tan\delta$ | $\varepsilon'_{max}$ | $T_m$ (K) | $\gamma$ | $C' \times 105$ (K) | $T_B$ (K) |
|--------|------|--------|---------|--------|--------|-----------|--------|
| Z05 | 1220 | 0.03 | 16054 | 533 | 1.4432 | 3.673 | 576 |
| Z10 | 1370 | 0.03 | 19066 | 546 | 1.4567 | 4.563 | 588 |
| Z15 | 1520 | 0.03 | 24085 | 555 | 1.4345 | 5.123 | 596 |
| Z20 | 1537 | 0.01 | 24488 | 557 | 1.5237 | 4.433 | 609 |
| Z25 | 1655 | 0.006 | 32900 | 575 | 1.7989 | 6.793 | 614 |
| Z30 | 1262 | 0.007 | 22789 | 579 | 1.8922 | 6.993 | 618 |

| Sample | $\varepsilon$ | tan δ | $\varepsilon'_{max}$ | $T_m$ (K) | $\gamma$ | $C' \times 105$ (K) | $T_B$ (K) |
|--------|------|--------|-----------------------|-----------|----------|----------------------|-----------|
| Z40 | 1001 | 0.012 | 18848 | 581 | 1.9241 | 5.77 | 620 |
| Z50 | 990 | 0.010 | 16541 | 582 | 1.9878 | 3.993 | 628 |
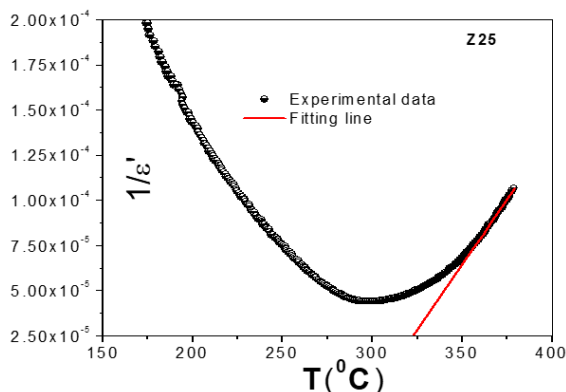


**Fig. 6.** Curie–Weiss dependence of the permittivity of the Z25 sample at temperatures much higher than $T_m$
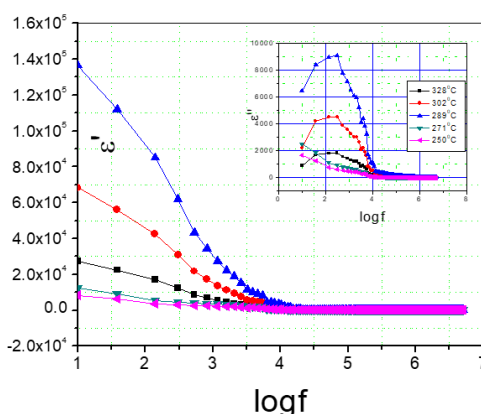


**Fig. 7.** Frequency dependence of real and imaginary part of dielectric permittivity of Z25 sample at different temperatures

## 3.4 Cole–Cole diagrams

Complex dielectric constant formalism is the most commonly used experimental technique to analyze the dynamics of the ionic movement in solids. The contribution of various microscopic elements, such as grain, grain boundary, and interface to total dielectric response in polycrystalline solids, can be identified from the reference to an equivalent circuit that contains a series of array and/or parallel RC elements [19].

To study the contribution originated from different effects, the Cole–Cole analyses were carried out at different temperatures.

It is observed that the dielectric constant data at low temperatures, i.e., up to about 289 °C, do not take the shape of a semicircle in the Cole–Cole plot but rather shows the straight line with a steep slope, suggesting the insulating behaviour of the compound at low temperatures. It could further be seen that with the increase in temperature, the slope of the lines decreases towards the real (ε′) axis and at temperatures above 289 °C, a semicircle could be traced (Fig. 8).
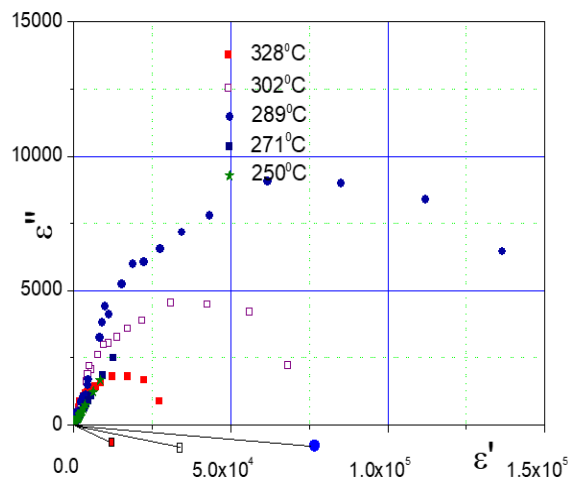


**Fig. 8.** Cole–Cole diagrams of Z25 sample at different temperatures

The Cole–Cole plot also provides information about the nature of the dielectric relaxation in the systems. For polydispersive relaxation, the plots are close to circular arcs with end points on the axis of real and the centre below this axis. The complex dielectric constant in such situations is described by the empirical relation:

$$\varepsilon^* = \varepsilon' - i\varepsilon'' = \varepsilon_\infty + \frac{\varepsilon_S - \varepsilon_\infty}{1 + (i\omega\tau)^{1-\alpha}} \qquad (3)$$

where $\varepsilon_s$ and $\varepsilon_\infty$ are the low- and high-frequency values of $\varepsilon$, and $\alpha$ is the measure of the distribution of relaxation times. The parameter $\alpha$ can be determined from the location of the centre of the Cole–Cole circles, of which only an arc lies above the $\varepsilon'$-axis [21]. It is evident from the plots that the relaxation process differs from the mono-dispersive Debye process (for which $\alpha = 0$). The parameter $\alpha$, as determined from the angle subtended by the radius of the circle with the $\varepsilon'$-axis passing through the origin of the $\varepsilon''$-axis [22-25], shows a slight increase in the interval [0.233, 0.187, 0.196] with a decrease of temperature from 601 to 562 K, implying a slight increase in the distribution of the relaxation time with decreasing temperatures below $T_m$.

## 4    Conclusions

In this paper, the effect of ZnO addition on the sintering behavior and dielectric properties of $0.9Pb(Zr_{0.49}Ti_{0.51})O_3–0.07Pb(Mn_{1/3}Nb_{2/3})O_3–0.03Pb(Sb_{1/2}Nb_{1/2})O_3$ ceramics is investigated. The addition of ZnO improves the sinterability of the materials and causes an increase in the density and grain size at a low sintering temperature (950 °C). The analysis of the microstructure evolution shows that the solubility limit of Zn ions in PZT–PMnN–PSbN systems is about 0.25% wt. At this concentration, the dielectric properties of ceramics appear to be the best with the following values: density 8.20 g/cm³, dielectric constant $\varepsilon_r = 1655$ and $\varepsilon_{max} = 32900$, and dielectric loss (tan$\delta$) 0.006. All samples have a pure perovskite phase, and the phase structure of the ceramics changes from rhombohedral to tetragonal with the increase in the ZnO content. The samples exhibit the relaxor behaviour with a diffuse phase transition with modeling of the dielectric data using modified Curie–Weiss law. The Cole–Cole plot also provides information about the nature of the dielectric relaxation in the systems.

## References

1. Smolenskii GA, Isupov VA, Agranovskaya AI. New Ferroelectrics of Complex Composition of the Type $A_2^{+2}(B_I^{3+}B_{II}^{5+})O_6$. Soviet physics Solid state. 1959;1:150-151.

2. Inoue A, Nguyen TT, Noda M, Okuyama M. Low temperature preparation of bismuth-related ferroelectrics by hydrothermal synthesis. In: 2007 Sixteenth IEEE International Symposium on the Applications of Ferroelectrics; 2007. p. 136-137.

3. Nguyen TT, Kanashima T, Okuyama M. Leakage current reduction and ferroelectric property of BiFe1-xCoxO3 thin films prepared by chemical solution deposition using rapid thermal annealing. MRS Proceedings; 2009:1199.

4. Tho NT, Inoue A, Noda M, Okuyama M, Low temperature preparation of bismuth-related ferroelectrics powder and thin films by hydrothermal synthesis. IEEE Trans Ultrasonic Ferroelec Freq Control. 2007; 54:2603-2607.

5. Truong-Tho N, Nghi-Nhan NT. Fabrication by annealing at approximately 1030°C and electrical characterization of lead-free (1-$x$)Bi0.5K0.5TiO3–$x$Ba(Fe0.5Nb0.5)0.05Ti0.95O3 piezoelectric ceramics. Journal of Electronic Materials. 2017;46(6):3585-3591.

6. Vuong LD, Tho NT. The Sintering bahavior and physical properties of Li2CO3-Doped Bi0.5(Na0.8K0.2)0.5TiO3 lead-free ceramics. International Journal of Materials Research. 2017;108(3):222-227.

7. Vuong LD, Truong-Tho N. Effect of ZnO nanoparticles on the sintering behavior and physical properties of Bi0.5(Na0.8K0.2)0.5TiO3 lead-free ceramics. Journal of Electronic Materials. 2017;46:6395-6402.

8. Tho NT, Kanashima T, Sohgawa M, Ricinschi D, Noda M, Okuyama M. Ferroelectric properties of Bi1.1Fe1-xCoxO3 thin films prepared by chemical solution deposition using iterative rapid thermal annealing in N2 and O2. Japanese Journal of Applied Physics. 2010;49:09MB05-7.

9. Truong-Tho N, Vuong LD. Sintering behavior and enhanced energy storage performance of SnO2 modified Bi0.5(Na0.8K0.2)0.5TiO3 lead-free ceramics. Journal of Electroceramics [Preprint]. 2020.

10. Tho NT, Kanashima T, Okuyama M. Leakage current reduction and ferroelectric property of BiFe1-xCoxO3 thin films prepared by chemical solution

deposition using iterative rapid thermal annealing at approximately 520°C. Japanese Journal of Applied Physics. 2010;49:095803-6.

11. Truong-Tho N, Vuong LD. Effect of sintering temperature on the dielectric, ferroelectric and energy storage properties of $SnO_2$-doped $Bi_{0.5}(Na_{0.8}K_{0.2})_{0.5}TiO_3$ lead-free ceramics. Journal of Advanced Dielectrics. 2020;10(04):2050011.

12. Vuong LD, Quang DA, Quan PV, Truong-Tho N. Fabrication of $Bi_{0.5}(Na_{0.4}K_{0.1})TiO_3$ lead-free ceramics using reactive templated grain growth method for improving their preferred degree of orientation, dielectric, and ferroelectric properties. Journal of Electronic Materials. 2020;49(11):6465-6473.

13. Gao F, Cheng L, Hong R, Liu J, Wang C, Tian C. Crystal structure and piezoelectric properties of $xPb(Mn_{1/3}Nb_{2/3})O_3$–$(0.2-x)Pb(Zn_{1/3}Nb_{2/3})O_3$–$0.8Pb(Zr_{0.52}Ti_{0.48})O_3$ ceramics. Ceramics International. 2009;35(5):1719-1723.

14. Vuong LD, Gio PD, Tho NT, Chuong TV. Relaxor ferroelectric properties of PZT-PZN-PMnN ceramics. Indian Journal of Engineering and Materials Sciences. 2014;20(22):555-560.

15. Luan NDT, Vuong LD, Chuong TV, Tho NT. Structure and physical properties of PZT-PMnN-PSN ceramics near the morphological phase boundary. Advances in Materials Science and Engineering. 2014;2014:1-8.

16. Tsai CC, Hong CS, Shih CC, Chu SY. Electrical properties and temperature behavior of ZnO-Doped PZT–PMnN modified piezoelectric. Journal of Alloys and Compounds. 2012 01;511(1):54-62.

17. Vuong LD, Gio PD. Effect of $Li_2CO_3$ Addition on the sintering behavior and physical properties of PZT-PZN-PMnN ceramics. International Journal of Materials Science and Applications. 2013;2(3):89-93.

18. Burns G, Dacol FH. Glassy polarization behavior in ferroelectric compounds $Pb(Mg_{1/3}Nb_{2/3})O_3$ and $Pb(Zn_{1/3}Nb_{2/3})O_3$. Solid State Communications. 1983;48(10):853-856.

19. Chen J, Chan HM, Harmer MP. Ordering structure and dielectric properties of undoped and La/Na-doped $Pb(Mg_{1/3}Nb_{2/3})O_3$. Journal of the American Ceramic Society. 1989;72(4):593-598.

20. Cole KS, Cole RH. Dispersion and absorption in dielectrics i. alternating current characteristics. The Journal of Chemical Physics. 1941 04;9(4):341-351.

21. Pirc R, Blinc R. Vogel-Fulcher freezing in Relaxor Ferroelectrics. Physical Review B. 2007;76(2).

22. He X, Zeng X, Zheng X, Qiu P, Cheng W, Ding A. Fabrication and characteristics of relaxor ferroelectric PZN-PZT (53/47) thin films by a MOD process. Journal of Physics: Conference Series. 2009;152:012068.

23. Setter N, Cross LE. The role of B-site cation disorder in diffuse phase transition behavior of perovskite ferroelectrics. Journal of Applied Physics. 1980;51(8):4356-4360.

24. Randall CA, Bhalla AS. Nanostructural-property relations in complex lead perovskites. Japanese Journal of Applied Physics. 1990;29(Part 1, No. 2):327-333.

25. Peláiz-Barranco A, González Abreu Y, López-Noda R. Dielectric relaxation and conductivity behavior in modified lead titanate ferroelectric ceramics. Journal of Physics: Condensed Matter. 2008;20(50):505208.